JOURNAL OF GUIDANCE, CONTROL, AND DYNAMICS
Vol. 34, No. 1, January–February 2011

Analytical Expressions that Characterize Propellantless Capture with Electrostatically Charged Spacecraft

Joseph W. Gangestad,* George E. Pollock,* and James M. Longuski†
Purdue University, West Lafayette, Indiana 47907-2045

DOI: 10.2514/1.47849

Spacecraft that intentionally maintain an electrostatic charge on their surface within a planetary magnetic field can manipulate the induced Lorentz force to perform propellantless maneuvers. Analytical expressions are developed that describe the process of capture with the Lorentz force and that demonstrate coupling among orbital elements (e.g., the eccentricity versus semilatus rectum) when the Lorentz force is the only perturbation on a Keplerian orbit. In equatorial orbits with a dipolar magnetic field, the relative evolution of the orbital elements notably depends on neither the charge nor on the magnetic field strength. The analytical solutions are applied to a capture at Jupiter, where, for example, a Galileo-like arrival requires ∼0.2 C/kg of charge to effect capture. The analytical solutions agree with numerical propagations to within a fraction of a percent. A previous study, which numerically explored the parameter space of the Jupiter capture problem, identified trends and constraints on the motion that can now be explained by the analytical theory.

Nomenclature

a	=	semimajor axis, km
$\mathbf{B}$	=	magnetic field vector, T
B_0	=	magnetic moment, T · km^3
C	=	retrograde-capture constant of integration
e	=	orbital eccentricity
$\mathbf{F}_G$	=	specific gravitational force vector, km/s^2
$\mathbf{F}_L$	=	specific Lorentz-force vector, km/s^2
h	=	specific orbital angular momentum, km^2/s^2
K	=	prograde-capture constant of integration
p	=	semilatus rectum, km
q	=	specific charge, C/kg
R_J	=	radius of Jupiter, km
R_{sync}	=	synchronous orbit radius, $(\mu/\omega_P^2)^{1/3}$, km
$\mathbf{r}$	=	position vector, km
$\hat{\mathbf{r}}$	=	radial unit vector
r	=	radial coordinate, km
r_p	=	radius of periapsis, km
T	=	specific kinetic energy, km^2/s^2
$\mathbf{v}$	=	inertial velocity vector, km/s
v	=	inertial velocity, km/s
$\mathbf{v}_{\text{rel}}$	=	velocity vector relative to magnetic field, km/s
v_∞	=	velocity at infinity, km/s
W	=	specific work, km^2/s^2
γ	=	dimensionless v_∞^2
δ	=	dimensionless charge variable
θ	=	polar coordinate, rad
$\hat{\boldsymbol{\theta}}$	=	polar unit vector
μ	=	gravitational parameter, km^3/s^2
ν	=	true anomaly, rad
ϕ	=	azimuthal coordinate, rad
$\hat{\boldsymbol{\phi}}$	=	azimuthal unit vector
$\boldsymbol{\omega}_P$	=	planetary rotation vector, rad/s
ω_P	=	planetary rotation rate, rad/s

Received 27 October 2009; revision received 3 September 2010; accepted for publication 3 September 2010.

*Ph.D. Candidate, School of Aeronautics and Astronautics, 701 West Stadium Avenue. Student Member AIAA.

†Professor, School of Aeronautics and Astronautics, 701 West Stadium Avenue. Associate Fellow AIAA.

Introduction

UNDER most circumstances, spacecraft charging is an undesirable side effect of operation in plasma-rich environments, such as in the vicinity of a planetary magnetic field. A number of technologies are incorporated into spacecraft design to mitigate this charge and to protect hardware from electromagnetic interference, arcing, and shorting [1]. If a sufficient charge is present, the spacecraft moving at orbital velocities in a magnetic field would be subject to a Lorentz force that perturbs the orbit in a significant way [2]. In this paper, we consider a hypothetical propellantless spacecraft, which we call a Lorentz spacecraft, that intentionally generates an electrostatic charge on its surface. Active modulation of this surface charge can manipulate the induced Lorentz force to modify or do work on the orbit, creating a source of propellantless thrust. Previous studies have found many potent applications for Lorentz spacecraft, including propellantless escape [3], stationkeeping [4], inclination change [5], rendezvous [6], J_2 cancellation [2], and low geosynchronous orbit [7].

The propulsive force of a Lorentz spacecraft is analogous to that of an electrodynamic (ED) tether. The current vector in a tether is crossed with the magnetic field to create a Lorentz force; the current of a Lorentz spacecraft is constrained to the direction of its velocity vector. Many applications require tethers several kilometers in length [8], but the use of electrostatic charge on a Lorentz spacecraft opens the possibility of compact construction [2]. The Lorentz spacecraft may therefore be treated as a charged point mass. Nonuniform charge distributions have been considered for the purpose of attitude control (by offsetting the spacecraft charge center from the center of mass and inducing a torque) [9], but the work developed here assumes a uniform electrostatic charge, thereby decoupling the attitude dynamics and orbital mechanics (not always possible with a tether) and simplifying the analysis. The relative performance of ED tethers and Lorentz spacecraft is considered later in the discussion section of this paper.

The key measure of a Lorentz spacecraft's ability to accelerate is its charge-to-mass ratio, or specific charge. Higher specific charges lead to higher accelerations from the Lorentz force and, therefore, to more effective maneuvers. The challenge of constructing a Lorentz spacecraft remains an open question, especially in the case of specific charges greater than a few hundredths of a coulomb per kilogram. Some of the hardware challenges have been laid out by Schaub et al. [10], by Peck [2], and by Choiniere and Gilchrist [11]. A number of options for charge generation have been proposed, and the development of a Lorentz spacecraft testbed is ongoing [12,13]. An upper limit on what may be considered a feasible specific charge is a matter of debate, but charge-to-mass ratios as

high as 0.001–0.01 C/kg have been proposed as possible in the next few decades, with a concerted research effort [14]. Given that Lorentz spacecraft are not likely to be fielded for some years, and in order to explore and exploit the full capabilities of these vehicles, we consider specific charges on the order of 0.01 C/kg to be acceptable and near-term feasible for applications, although present-day technology may preclude the generation of such a charge magnitude. The physical architecture of a Lorentz spacecraft also remains speculative. It shall be assumed that the vehicle is compact and does not employ kilometer-long filaments or other large components, as has been suggested for some variants of the technology [14].

Propellantless capture at Jupiter has become an attractive application for Lorentz spacecraft because of the ostensibly near-term feasible specific charges necessary to effect capture. Recently, Atchison and Peck performed a thorough numerical analysis of the capture problem at Jupiter [15]. They used a two-body drag-free system confined to equatorial orbits, and they numerically propagated the equations of motion, using a bang–off charge-control scheme to lower the orbital energy and to achieve capture. By propagating over 1000 different initial orbits at four different specific charge levels, they identified orbits that capture, impact, and flyby, and they characterized those orbits by the time necessary to achieve a desired final state. Streetman and Peck considered an analytical approach to planetary capture with Lorentz spacecraft [16], but they used orbit-averaged equations to facilitate their investigation into planetary flyby augmentation, the primary topic of their paper.

In this paper, we develop an analytical treatment of the equatorial capture problem for Lorentz spacecraft. The analytical solutions that are derived here apply to all stages of the capture and postcapture process and confirm the numerical results of Atchison and Peck. Earlier analytical work with electrostatically charged spacecraft has primarily considered the regime of natural spacecraft charging, where the specific charges achieved do not typically exceed 10^{-8} C/kg [17]. Although such a charge (corresponding to potentials at GEO as high as several kilovolts) may adversely impact the functions of hardware, from an orbital dynamics perspective, the contribution of the Lorentz force can be neglected [18]. At the other extreme, physicists and astronomers have published substantial work on the dynamics of charged dust, such as in Saturn's rings. Dust particles in space develop specific charges of hundreds or thousands of coulombs per kilogram, sometimes high enough to neglect even the gravitational force [19,20].

Lorentz spacecraft maintain a specific charge between these extremes, so that the Lorentz force acts as a small but significant perturbation on the Keplerian orbit. The Lorentz force that affects ED tethers has been studied extensively [21–23], but consideration of electrostatically charged spacecraft at the same acceleration levels has been sparse until only recently [2,24,25]. At this early stage of investigation, where the search for unique and relevant applications of Lorentz spacecraft is ongoing, it is prudent to search for analytical solutions to both general and specific problems. If they are available, closed-form solutions allow for immediate and broad insight into the dynamical behavior. The analytical work developed here is intended to provide a first-order assessment of the Lorentz-force effects on a Keplerian orbit during and after capture.

Analytical Solutions

Modeling the Lorentz Force for Capture

The magnetic field of a planet can be approximated to the first order by that of a perfect dipole with the origin at the center of the planet. The dipole is aligned with the planetary rotation axis and rotates uniformly with the planet. It has been shown that the small tilt of the magnetic fields of Earth and Jupiter does not cause a substantial deviation of the motion from the untilted case [3,7]. Figure 1 defines the Cartesian (x, y, z) and spherical polar (r, θ, ϕ) coordinates (in an inertial reference frame) that are used throughout this paper. The origin of both coordinate systems is at the center of the planet and dipole, and the vector $\mathbf{r}$ points from the origin to the Lorentz spacecraft. The Cartesian z axis is aligned with the planet's rotation axis; the polar angle θ is measured from the z axis and the azimuthal angle ϕ from the x axis. Because the dipolar magnetic field is axisymmetric and independent of longitude, the inertial orientation of the x and y axes is arbitrary. All integrations and analyses are performed with either polar coordinates or orbital elements; the Cartesian coordinates in Fig. 1 are not used beyond providing a reference for the reader in defining the angles of the polar coordinate system.

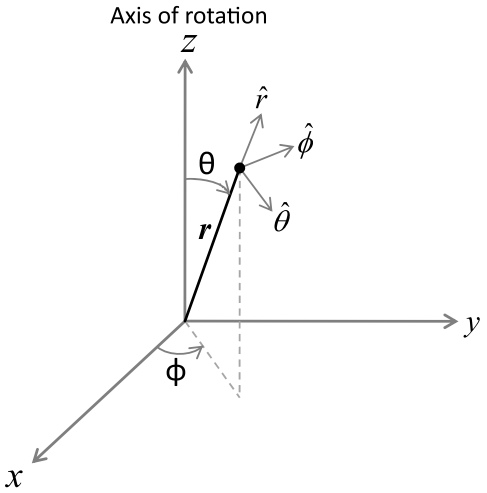

Fig. 1 Inertial Cartesian and spherical polar coordinates, with the origin at the center of the planet and dipole.

The Lorentz force is given by

$$\mathbf{F}_L = q\mathbf{v}_{\text{rel}} \times \mathbf{B} = q(\mathbf{v} - \boldsymbol{\omega}_P \times \mathbf{r}) \times \mathbf{B} \tag{1}$$

The force depends on the velocity relative to the magnetic field; taking the time derivative of the position vector with respect to the noninertial rotating frame of the planet and magnetic field introduces an additional $\boldsymbol{\omega}_P \times \mathbf{r}$ that must be subtracted from the inertial velocity $\mathbf{v}$. The magnetic field of a perfect dipole is given by [26]

$$\mathbf{B} = (B_0/r^3)(2\cos\theta\hat{\mathbf{r}} + \sin\theta\hat{\boldsymbol{\theta}}) \tag{2}$$

Incorporation of Eq. (2) into Eq. (1) and a point-mass gravity model leads (after some algebra, as addressed in other treatments [4,7]) to the equations of motion,

$$\ddot{r} - r\dot{\theta}^2 - r\dot{\phi}^2\sin^2\theta + \mu/r^2 + (qB_0\sin^2\theta/r^2)(\dot{\phi} - \omega_P) = 0 \tag{3a}$$

$$r\ddot{\theta} + 2\dot{r}\dot{\theta} - r\dot{\phi}^2\sin\theta\cos\theta - 2(qB_0\sin\theta\cos\theta/r^2)(\dot{\phi} - \omega_P) = 0 \tag{3b}$$

$$\frac{\mathrm{d}}{\mathrm{d}t}[r^2\dot{\phi}\sin^2\theta + qB_0(\sin^2\theta/r)] = 0 \tag{3c}$$

where a typographical error in Eq. (3b) by Gangestad et al. [4] has been corrected. These differential equations are numerically integrated later as a truth model to validate the analytical solutions that are subsequently developed.

In a capture scenario, the most popular (and time optimal [15]) control for the specific charge has been a bang–bang scheme, where the charge polarity is switched every half orbit, or a bang–off scheme, where the charge is on for half of an orbit and off for the other half. Figure 2 shows the gravity and Lorentz-force vectors acting on a spacecraft in an equatorial hyperbolic orbit moving in a counterclockwise direction. The spacecraft in the figure employs the bang–bang control, as evidenced by the change in sign of the charge from $+q$ to $-q$. The figure shows a view from above, and the magnetic field in the equatorial plane is directed into the page. The depicted magnetic field corresponds to Jupiter and Saturn; at Earth, the field would be directed out of the page and capture would require the opposite charge polarities.

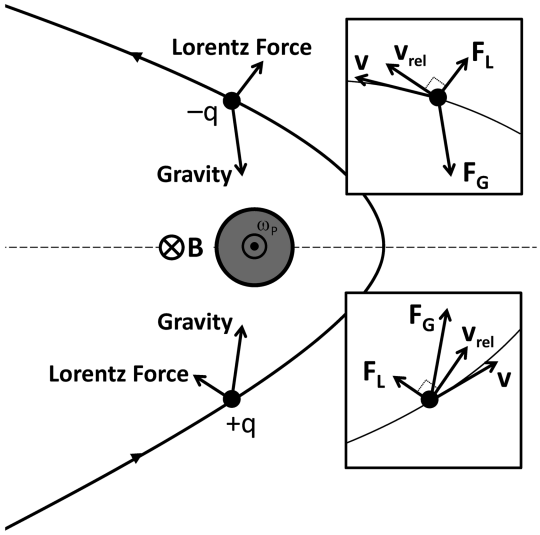

Fig. 2 A Lorentz spacecraft (moving counterclockwise) in an equatorial hyperbolic orbit, employing a bang–bang control scheme to effect capture by doing negative work and reducing the orbital energy.

The insets in Fig. 2 show the gravitational force $\mathbf{F}_G$, the inertial velocity $\mathbf{v}$ of the Lorentz spacecraft, the velocity relative to the magnetic field $\mathbf{v}_{\text{rel}}$, and the resulting Lorentz force $\mathbf{F}_L$. $\mathbf{F}_L$ is orthogonal to $\mathbf{v}_{\text{rel}}$ (because the Lorentz force is perpendicular to both the relative velocity and the magnetic field) but not to $\mathbf{v}$. To capture at the planet, the orbital energy must be decreased. To do negative work, the work-energy theorem, $\dot{W} = \mathbf{F} \cdot \mathbf{v}$ [also see Eq. (15) et seq.], implies that the projection of the Lorentz force onto the inertial velocity must be negative. The choice of positive charge during descent and the negative charge during ascent ensures that $\mathbf{F}_L \cdot \mathbf{v}$ is negative, doing negative work and reducing the orbital energy. If the orbit were inclined, the same vectorial argument would apply, but any out-of-plane component of the Lorentz force would contribute to a change in inclination or to nodal precession. In a bang–off scheme, this control is implemented for half of the orbit; for example, the charge is on for the inbound portion of the hyperbola and then deactivated (i.e., q set to zero) after periapsis passage. After capture, the orientation of the vectors remains similar, and the same control can be used over many orbits to lower the now-elliptical orbit to a desired altitude [3]. Because the Lorentz force is available only half as often in the bang–off control, it is expected that maneuvers and orbit lowering with the bang–off scheme would take twice as long to complete.

No single orbital element can be manipulated independently (except for some instantaneous cases, such as changing the semimajor axis independently when the eccentricity is zero [3]). The bang–bang and bang–off control schemes change the orbital energy and, hence, the semimajor axis, but the effects of the transverse components of the Lorentz force on eccentricity, inclination, and other orbital elements are not immediately obvious. It is possible, for example, that changes to eccentricity could be deleterious and lead to impact with the planet. Therefore, it is necessary to understand how the other orbital elements evolve during the capture process and to assess the feasibility of capture (subject to physical and technological constraints) in the entire space of possible initial conditions.

In the case of propellantless capture, it is advantageous to use orbital elements, rather than polar coordinates, as dynamical variables. The evolution of the Cartesian or polar coordinates is determined by the nonlinear equations of motion, and each coordinate changes rapidly with time; the orbital elements tend to evolve more slowly, and there is often only one fast variable (e.g., the true anomaly). Gangestad et al. [3] incorporated the Lorentz force of Eq. (1) into Lagrange's planetary equations, deriving general expressions for the time rate of change of the orbital elements given a perturbing Lorentz force. The bang–bang and bang–off control laws employed by Lorentz spacecraft are typically selected with the growth of a single orbital element (frequently the semimajor axis) in mind, so that one can treat that orbital element as tunable itself (although the other elements may behave in unexpected or undesirable ways). Given such a control over one orbital element, it is preferable to study the relative evolution of the orbital elements rather than their propagation in time.

Evolution of Orbital Elements

In Gangestad et al. [3], propellantless escape from an equatorial orbit is considered, and the effect of the Lorentz force on the relative evolution of the semimajor axis and eccentricity is assessed. In particular, analytical expressions were found for the reachable sets of orbits given an arbitrary initial orbit, and regions of circularizability and escapability were identified. However, for that analysis, the validity of the analytical expressions is limited to bound orbits. In the case of capture, one must consider both hyperbolic and elliptical orbits, and care must be taken in the transition between the two regimes. The use of the semimajor axis as an orbital element for the capture case is problematic because of its discontinuity at the parabolic orbit. As the Lorentz force manipulates the orbital eccentricity through unity from a hyperbolic to an elliptical orbit, reliance on the semimajor axis can lead to divisions by zero and indeterminate forms in the analysis. Instead of the semimajor axis, we use the semilatus rectum and the eccentricity, both of which are positive and continuous across hyperbolic, parabolic, and elliptical orbits, to evaluate the capture process.

The semilatus rectum is related to the orbital angular momentum by the relation,

$$p = h^2/\mu \tag{4}$$

and its time derivative may be written as

$$\dot{p} = (2/\mu)h\dot{h} \tag{5}$$

The Lorentz force perturbs the orbital angular momentum, and so we may rewrite Eq. (5) with expressions for $\dot{h}$ in an equatorial orbit, as found by Gangestad et al. [3],

$$\dot{p} = (2/\mu)qB_0 h r\dot{\phi} = 2(qB_0/p^2)e \sin\nu(1 + e\cos\nu)^2 \tag{6}$$

in agreement with Streetman and Peck [16], where the choice of positive sign for $\dot{\phi}$ implicitly assumes prograde orbits. The case of retrograde orbits is briefly addressed later. The change in eccentricity from the Lorentz force is given by [3]

$$\dot{e} = -(qB_0/p^3)\sin\nu(1 + e\cos\nu)^2[(1 - e^2) - \omega_P\sqrt{p^3/\mu}] \tag{7}$$

for equatorial orbits. The fast variable in this treatment of Lagrange's planetary equations is the true anomaly. The terms containing the true anomaly in Eqs. (6) and (7) are the same, and division of the latter equation by the former eliminates the true anomaly, leaving

$$\mathrm{d}e/\mathrm{d}p = [-1/(2ep)][(1 - e^2) - \omega_P\sqrt{p^3/\mu}] \tag{8}$$

a differential equation that contains only the variables p and e (and known constants). The singularity at $p = 0$ corresponds to a rectilinear orbit, which would exist only instantaneously if the Lorentz force were applied to modify the orbit. Also, the upcoming analysis demonstrates that circularization is an asymptotic process, such that in the applications considered here, the singularity at $e = 0$ is never reached. The solution to the differential equation in Eq. (8) describes the relative evolution of the two orbital elements. Both the charge and the magnetic moment have dropped out of Eq. (8), indicating that the relative evolution of p and e is independent of the control (i.e., q) and of the magnetic field strength (i.e., B_0). Instead, the manner in which p and e change with respect to one another is intrinsic to the introduction of the perturbing Lorentz force.

To generalize the analysis, we scale the semilatus rectum (and all other variables with dimension of length) by the synchronous orbital radius, so that by writing

$$\bar{p} = p/R_{\text{sync}} = p/(\mu/\omega_P^2)^{1/3} \tag{9}$$

we may rewrite Eq. (8) as

$$\mathrm{d}\,e/\mathrm{d}\bar{p} = [-1/(2e\bar{p})][(1-e^2) - \bar{p}^{3/2}] \tag{10}$$

Any variable that has been scaled by the synchronous radius in the manner of Eq. (9) is denoted by a bar over the variable.

The differential equation in Eq. (10) has the closed-form solution,

$$e(\bar{p}) = \sqrt{1 + 2\bar{p}^{3/2} + K\bar{p}} \tag{11}$$

where K is a unitless constant of integration given by

$$K = (1/\bar{p}_0)(e_0^2 - 1 - 2\bar{p}_0^{3/2}) \tag{12}$$

The argument of the square root in $e(\bar{p})$ remains positive for all e_0, $p_0 > 0$. Equation (11) describes how the orbital eccentricity changes as the Lorentz force manipulates the semilatus rectum. The bang–bang and bang–off control laws applied by a Lorentz spacecraft are usually designed to grow or shrink the semimajor axis, but in this case, p is used in place of the semimajor axis. Equation (11) provides no insight into the design of a particular control to grow or shrink p; that is a substantial topic outside the scope of this paper. Instead, the relation reveals how the eccentricity is affected as the semilatus rectum changes. Because Eq. (11) contains no term with q or B_0, this relative evolution is independent of both the control and the planetary magnetic properties. This conclusion is true for equatorial orbits, which are considered here, but we note that, for inclined orbits, the behavior of the orbital elements can be control dependent [3].

Plots of Eq. (11) appear in Fig. 3. Every point on the plot represents a possible initial orbit. Through any orbit, Eq. (11) draws a contour, which is the reachable set of orbits for all orbits on the contour. Given some initial equatorial orbit [which determines the value of K in Eq. (11)], the Lorentz force can transform that initial orbit only to orbits along its corresponding contour. The bold line corresponds to the contour that contains the synchronous orbit ($\bar{p} = 1$ and $e = 0$, where $K = -3$). This contour creates a boundary between classes of orbits. Below the line, the reachable sets contain $e = 0$, indicating that the orbits along these contours are circularizable [3]. Above the threshold, the orbits are noncircularizable. In the region of orbits below the bold line with $p < 1$ and $e < 1$, the reachable sets remain confined to that triangular region. No application of the Lorentz force can drive these orbits to become parabolic or hyperbolic ($e \geq 1$); therefore, they are characterized as inescapable. Conversely, then, no initially hyperbolic orbits exist that can be captured into orbits in this region. The lowest possible circular orbit that a capture scenario can achieve is at the synchronous radius (by choosing an initial condition on the bold line). All other captures that lead to circular orbits (above the synchronous radius) are below and to the right of the bold line; those that lead to elliptical orbits are above the bold line. Incoming

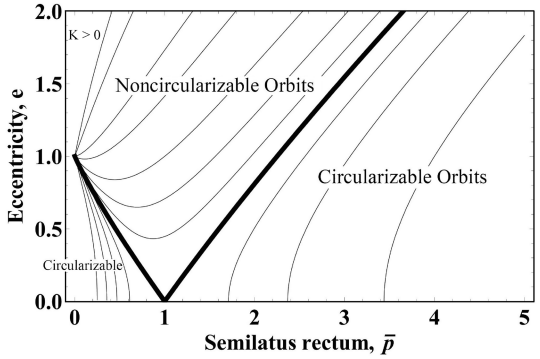

Fig. 3 The evolution of orbital eccentricity versus dimensionless semilatus rectum via the Lorentz force for several different initial orbits. The bold line (where $K = -3$), which includes the synchronous orbit, separates circularizable and noncircularizable orbits.

hyperbolic orbits that are noncircularizable achieve a minimum eccentricity, which can be calculated from the derivative of Eq. (11),

$$\frac{\mathrm{d}(e^2)}{\mathrm{d}\bar{p}} = 3\bar{p}^{1/2} + K = 0 \tag{13}$$

which implies [by substitution of the solution of Eq. (13) back into Eq. (11)] that

$$e_{\min} = 1 + (1/27)K^3 \tag{14}$$

Only orbits with $-3 < K < 0$ have this minimum; orbits with $K \leq -3$ are circularizable, and the minimum eccentricity lies at the end of the domain (i.e., at $e = 0$) and, for orbits with $K > 0$, Eq. (13) has no solution for positive $\bar{p}$. Noncircularizable orbits have a minimum eccentricity, because the differential de changes sign before $e = 0$ [3]; the charge control may continue to extract energy from the orbit (lowering the semimajor axis), but the eccentricity begins to rise after this sign change, and the periapsis drops substantially.

Figure 3 offers no information regarding the time scales of this notional circularization or a possible control to affect it; rather, Fig. 3 provides a guide (akin to a Tisserand graph [27]) for assessing the feasibility of possible mission profiles. For example, from Fig. 3 we conclude that propellantless capture with a Lorentz spacecraft into low circular orbits is not possible (independent of control law), because those low orbits (in the lower left triangular region below the bold line) are not contained in the reachable sets of any initially hyperbolic orbits.

For initial orbits where $K > 0$ (i.e., $e_0^2 > 1 + 2\bar{p}_0^{3/2}$), in the upper left corner of Fig. 3, the contours never extend below $e = 1$, implying that there may be a set of orbits that cannot be captured. These extremely energetic orbits typically have nonphysical radii of periapsis (i.e., close to the singularity of the gravitational field) or require an infeasibly high specific charge for capture. In either case, the acceleration from the Lorentz force is high, sometimes exceeding that of gravity, such that the assumption of small perturbations breaks down, and Lagrange's planetary equations poorly model the evolution of the orbital elements. Therefore, examples where $K > 0$ (i.e., where the analytical theory is no longer valid) are not considered.

Expressions for Capture

To investigate the capture process itself, it is assumed that the Lorentz spacecraft uses a bang–off control, such that the vehicle turns off its charge after passing periapsis. On the inbound segment of the hyperbolic orbit, the Lorentz spacecraft maintains the appropriate constant charge to lose orbital energy. After periapsis, the charge is deactivated, and the spacecraft continues on a Keplerian trajectory. If the Lorentz force does not extract sufficient energy by periapsis passage, the orbit remains hyperbolic and the capture fails; therefore, it is of great interest to ascertain, for example, what specific charge is necessary to capture for a given set of initial conditions. To answer this question, one must understand how the initial conditions, specific charge, and planetary magnetic properties affect the final orbit.

According to the work-energy theorem, the total work done by the applied forces (in this case, the gravitational and Lorentz forces) equals the change in kinetic energy:

$$W = \int \mathbf{F} \cdot \mathbf{v}\,\mathrm{d}t = \Delta T \tag{15}$$

Using

$$\mathbf{F}_G = -\mu\hat{\mathbf{r}}/r^2 \tag{16}$$

for the gravitational force and incorporating Eq. (1), Eq. (15) can be written as

$$W = \int_\infty^r \left[-\frac{\mu\hat{\mathbf{r}}}{r^2} + q(\mathbf{v} - \boldsymbol{\omega}_P \times \mathbf{r}) \times \mathbf{B}\right] \cdot \mathbf{v}\,\mathrm{d}t = \frac{1}{2}v^2 - \frac{1}{2}v_\infty^2 \tag{17}$$

where the spacecraft begins at infinity and descends to some radius r. In the equatorial plane (i.e., $\theta = \pi/2$),

$$\boldsymbol{\omega}_P = -\omega_P \hat{\boldsymbol{\theta}} \tag{18}$$

and [from Eq. (2)]

$$\mathbf{B} = (B_0/r^3)\hat{\boldsymbol{\theta}} \tag{19}$$

so that

$$[q(\mathbf{v} - \boldsymbol{\omega}_P \times \mathbf{r}) \times \mathbf{B}] \cdot \mathbf{v}\, \mathrm{d}t = \frac{qB_0\omega_P}{r^2}\dot{r}\, \mathrm{d}t = \frac{qB_0\omega_P}{r^2}\, \mathrm{d}r \tag{20}$$

where the inertial velocity is given by

$$\mathbf{v} = \dot{r}\hat{\mathbf{r}} + r\dot{\theta}\hat{\boldsymbol{\theta}} + r\dot{\phi}\sin\theta\hat{\boldsymbol{\phi}} \tag{21}$$

Substituting Eq. (20) into Eq. (17) yields

$$\begin{aligned} W &= \int_\infty^r \left(-\frac{\mu}{r^2} + \frac{qB_0\omega_P}{r^2}\right)\mathrm{d}r = -\mu\left(1 - \frac{qB_0\omega_P}{\mu}\right)\int_\infty^r \frac{\mathrm{d}r}{r^2} \\ &= \frac{\mu}{r}\left(1 - \frac{qB_0\omega_P}{\mu}\right) \end{aligned} \tag{22}$$

The Lorentz force has the effect of modifying the effective gravitational parameter of the planet (all of the terms in parentheses are constants), and the appropriate choice of charge polarity can either increase or decrease its apparent mass. By substituting the vis viva equation,

$$v^2/2 - \mu/r = -\mu/(2a) \tag{23}$$

into Eq. (17) to eliminate v^2, and using Eq. (22), the semimajor axis of the orbit at radius r is given by

$$a = \mu(2qB_0\omega_P/r - v_\infty^2)^{-1} \tag{24}$$

that, in terms of the semilatus rectum and eccentricity, is

$$p(2qB_0\omega_P/r - v_\infty^2) = 1 - e^2 \tag{25}$$

To nondimensionalize Eq. (25), we define

$$\delta \equiv qB_0\omega_P/\mu \tag{26}$$

and

$$\gamma \equiv v_\infty^2 R_{\mathrm{sync}}/\mu \tag{27}$$

so that we may now write Eq. (25) as

$$\bar{p}(2\delta/\bar{r} - \gamma) = 1 - e^2 \tag{28}$$

The assumption of a bang–off control scheme is consistent with that made by Atchison and Peck in their numerical investigation of the problem [15]. However, in their work, the bang–off control switches in the opposite order; they assume the charge is activated after periapsis passage (to allow for a more hardware-amenable charge polarity). Turning on the charge after periapsis is not as readily incorporated into the analytical model, because the final apoapsis altitude of the captured orbit is not known a priori; evaluation of the work integral would require two finite bounds, whereas in our treatment, having one of the bounds at infinity simplifies the final expressions. The symmetry of the magnetic dipole field in the equatorial plane will lead to very similar results, although some small numerical differences may arise, because the bounds on the work integrals differ.

When the charge on the Lorentz spacecraft turns off at periapsis, $\bar{r} = \bar{r}_p$ and, at that point, it remains to be determined whether the orbit has been successfully captured. In particular, we must solve for $\bar{p}$ and e at $\bar{r}_p$; however, because the Lorentz force transforms the orbital elements throughout the motion down to periapsis, the value of $\bar{r}_p$ changes as well, so that the variable must also be solved for simultaneously. Fortunately, the well-known relation for $\bar{r}_p$,

$$\bar{r}_p = \bar{p}/(1 + e) \tag{29}$$

is continuous at all eccentricities. Evaluating Eq. (28) at $\bar{r}_p$ gives

$$\bar{p}(2\delta/\bar{r}_p - \gamma) = 1 - e^2 \tag{30}$$

so that, for the three unknowns $\bar{p}$, e, and $\bar{r}_p$, there are three Eqs. (11), (29), and (30). After some algebra, one arrives at an algebraic expression for $\bar{p}$ at periapsis

$$\begin{aligned} &4\bar{p}^2 + 4(K - \gamma)\bar{p}^{3/2} + (K - \gamma)^2\bar{p} + 8\delta(1 - \delta)\bar{p}^{1/2} \\ &\quad + 4\delta[K(1 - \delta) - \gamma] = 0 \end{aligned} \tag{31}$$

which is solvable as a quartic polynomial in $\bar{p}^{1/2}$. Although the quartic polynomial has a general solution, the final expression for $\bar{p}$ contains dozens of terms, including many square and cube roots, and does not offer any insight. We can find adequate solutions for the three unknowns by approximation methods that do not require cumbersome, lengthy expressions. We have observed anecdotally that, over the course of the capture process (when the integrations use a specific charge less than ~0.1 C/kg at Jupiter, which in turn leads to low perturbative accelerations from the Lorentz force), all three of $\bar{p}$, e, and $\bar{r}_p$ differ little at periapsis from their initial values at infinity (at most, a few percent typically). Over several orbits, the orbital elements can be changed dramatically, but for the single pass necessary to accomplish capture, the change is proportionally small. Therefore, it is assumed that

$$\bar{p} = \bar{p}_0(1 + \eta) \tag{32a}$$

$$e = e_0(1 + \zeta) \tag{32b}$$

$$\bar{r}_p = \bar{r}_{p0}(1 + \epsilon) \tag{32c}$$

where $|\eta|$, $|\zeta|$, and $|\epsilon| \ll 1$, and that the initial orbital elements $\bar{p}_0$, e_0, and $\bar{r}_{p0} = \bar{p}_0/(1 + e_0)$ are known. Substituting Eq. (32a) into Eq. (11) and Taylor-expanding to linear order in η yields

$$e^2 \approx e_0^2 + (3\bar{p}_0^{3/2} + K\bar{p}_0)\eta \tag{33}$$

Similar substitutions of Eqs. (32a–32c) into Eqs. (11), (29), and (30) and linearization around the small variations lead ultimately to

$$\eta = -\frac{2\delta(1 + e_0)}{\bar{p}_0^{3/2} + (\bar{p}_0^{3/2} + e_0^2 - 1)(\delta/e_0)} \tag{34}$$

where

$$e^2 = e_0^2 - \frac{2\delta(1 + e_0)(\bar{p}_0^{3/2} + e_0^2 - 1)}{\bar{p}_0^{3/2} + (\bar{p}_0^{3/2} + e_0^2 - 1)(\delta/e_0)} \tag{35}$$

at periapsis, where K is eliminated via Eq. (12). Similarly, the radius of periapsis is given by

$$\bar{r}_p = \bar{p}/(1 + e) = \bar{p}_0(1 + \eta)\left[1 + \sqrt{e_0^2 + (\bar{p}_0^{3/2} + e_0^2 - 1)\eta}\right]^{-1} \tag{36}$$

Inspection of Eqs. (32a) and (34–36) permits the characterization of the growth or reduction of the orbital elements according to the sign of δ during the capture process. The orbital elements at periapsis depend on η. Table 1 shows the relationship between η and the charge δ, assuming that $\bar{p}_0 > 0$ and $e_0 > 1$ (i.e., initially hyperbolic). The second line of the table shows a region of negative δ, where η is positive. The nonzero bound of δ on that region tends to be a negative number of order one; a $\delta \approx -1$ corresponds to specific charges of 1–1000 C/kg at Earth, Jupiter, or Saturn, far beyond the charges that are considered feasible or valid for this analysis. We do not expect to

Table 1 Relationship between δ and η

Range of δ	η
$\delta > 0$	$\eta < 0$
$-e_0\bar{p}_0^{3/2}/(\bar{p}_0^{3/2} + e_0^2 - 1) < \delta < 0$	$\eta > 0$
$\delta < -e_0\bar{p}_0^{3/2}/(\bar{p}_0^{3/2} + e_0^2 - 1)$	$\eta < 0$

Table 2 Orbital elements at periapsis versus initial values

$\eta > 0(\delta < 0)$	$\eta < 0(\delta > 0)$	Note
$\bar{p} > \bar{p}_0$	$\bar{p} < \bar{p}_0$	
$e > e_0$	$e < e_0$	
$\bar{r}_p > \bar{r}_{p0}$	$\bar{r}_p < \bar{r}_{p0}$	$K > -3$
$\bar{r}_p < \bar{r}_{p0}$	$\bar{r}_p > \bar{r}_{p0}$	$K < -3$

encounter the region of negative δ beyond that bound where η returns to negative values (in the third line of the table), and so in practice, it is reasonable to assume that negative δ leads to positive η and vice versa.

Table 2 shows the relationship of the orbital elements at periapsis to their initial values depending on the sign of η and, in the case of the periapsis radius, on K. For capture, we require a decrease in eccentricity at periapsis, $e < e_0$ that, according to Table 2, requires $\delta > 0$. The nondimensional δ must be positive for capture, so the polarity of the specific charge q must change, depending on the magnetic properties of the planet to maintain that sign on δ (recalling that $\delta \equiv qB_0\omega_P/\mu$, where B_0 can be positive or negative). Therefore, Table 2 implies that the semilatus rectum always decreases during the capture process; this effect can also be deduced from Fig. 3, where the slopes of the contours show a direct relationship between e and $\bar{p}$ when the initial eccentricity is greater than one. The radius of the periapsis during capture can either increase or decrease, depending on the initial conditions. The change depends on the initial orbital elements: if $K > -3$ (i.e., corresponding to noncircularizable orbits above the bold line in Fig. 3), the radius of periapsis decreases during capture; if $K < -3$, the radius of periapsis increases. The analytical theory implies that $K = -3$ corresponds to orbits for which the periapsis remains constant; in practice, the nonlinearity of the problem leads to some change in periapsis even when initially $K = -3$.

A capture has occurred when the eccentricity at periapsis [as given by Eq. (35)] is less than unity. Setting $e^2 < 1$ isolates δ, the minimum charge necessary to effect the capture. The denominator of Eq. (35) is positive for initially hyperbolic orbits (i.e., $e_0 > 1$) and $\delta > 0$, so that for $e^2 < 1$,

$$\delta > \frac{\bar{p}_0^{3/2}(e_0^2 - 1)}{[2(1 + e_0) - (e_0^2 - 1)/e_0](\bar{p}_0^{3/2} + e_0^2 - 1)} = \frac{\bar{r}_{p0}^2\gamma(1 + \bar{r}_{p0}\gamma)}{2\bar{r}_{p0} + \bar{r}_{p0}^2\gamma + \gamma\sqrt{2\bar{r}_{p0} + \bar{r}_{p0}^2\gamma}} \tag{37}$$

We have expressed δ in terms of $\bar{r}_{p0}$ and γ (the nondimensional v_∞) because, in practice, flybys are seldom designed via p_0 and e_0. Figure 4 shows four plots with contours of Eq. (37), the minimum charge necessary for capture, versus the initial radius of periapsis and v_∞. The upper left plot shows the nondimensional δ contours versus $\bar{r}_{p0}$ and γ, whereas the other three plots show the specific charge q contours versus the dimensional r_{p0} and v_∞ for Earth, Jupiter, and Saturn. The axes for Earth are more restricted than for Jupiter and

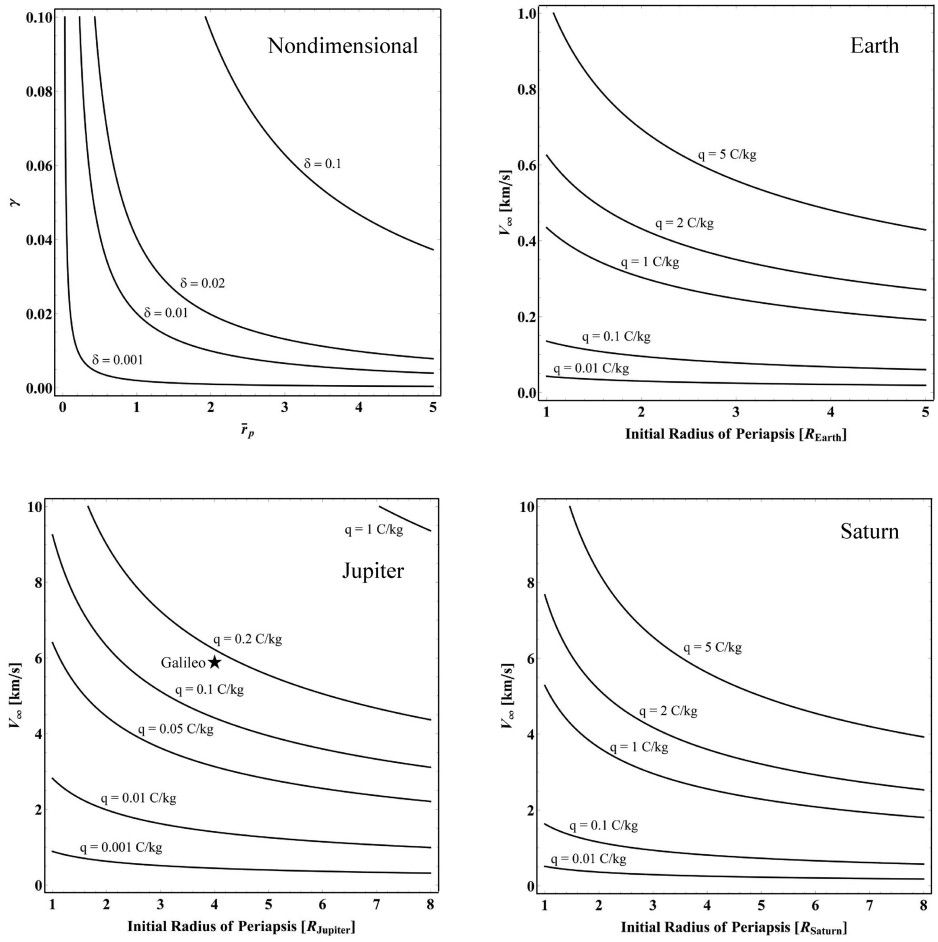

Fig. 4 Contours of the minimum charge necessary for capture in nondimensional units and in dimensional units at Earth, Jupiter, and Saturn as a function of the initial radius of periapsis and v_∞.

Table 3 Planetary physical properties (normalized to Earth)

	Gravitational parameter, μ [a]	Magnetic moment, B_0 [b]	Rotation period [c]	Equatorial radius [d]
Earth	1	−1	1	1
Jupiter [e]	317.8	2×10^4	0.41	11.2
Saturn [e]	95.2	600	0.44	9.4

[a]Reference gravitational parameter of Earth: 398, 600 km^3/s^2
[b]Reference dipole moment of Earth: 8×10^6 T·km^3.
[c]Reference rotation period of Earth: 24 h.
[d]Reference radius of Earth: 6378 km.
[e]Values adapted from Connerney [28].

Saturn because of Earth's substantially weaker magnetic field and slower rotation. The magnetic properties used for each planet appear in Table 3. Lower minimum-charge contours appear in the lower left areas of each plot. The cases of low periapsis or small v_∞ correspond to low specific charge for capture. In the former case, a low periapsis leads to a high velocity during the flyby. The Lorentz force is proportional to the velocity of the spacecraft, so high velocity induces a strong impulsive Lorentz force at periapsis. In the latter case, a low incoming v_∞ leads to a slower flyby pass within the magnetic field, increasing the total time-integrated Lorentz force (although the lower velocity decreases the instantaneous magnitude of the force). In cases where both the periapsis and v_∞ are relatively high, the spacecraft passes through weaker parts of the magnetic field and for less time, demanding a higher charge for capture.

In nearly all cases, near-term-feasible captures (i.e., using 0.001–0.01 C/kg) require very low v_∞. At Earth and Saturn, only a near-parabolic arrival could capture at these charge levels. Jupiter can accommodate a few kilometers per second of v_∞ if the radius of periapsis is low. At all three planets, the gradient of the minimum-charge contours is greatest with changing v_∞. In a mission-design scenario, then, except for near-surface flybys, the best way to reduce charge-generation demands on the Lorentz spacecraft is to reduce the v_∞ as much as possible. The magnetic field drops off as r^{-3}, so most gains from low r_p occur only close to the origin, typically below the planet's surface. The tall vertical asymptotes in the nondimensional plot at the upper left of Fig. 4 are physically inaccessible at Earth, Jupiter, and Saturn. At Jupiter, the low-v_∞ arrivals that are near-term feasible at $q \approx 0.01$ C/kg are available only at very low perijoves and correspond to the v_∞ of a Hohmann transfer. Jupiter remains the most promising candidate for Lorentz spacecraft capture, but the interplanetary cruise must either include a low arrival periapsis or employ low thrust or some other nonconventional propulsion method to ensure a low arrival v_∞. The incorporation of a low-thrust system for interplanetary travel does not necessarily negate the capture and orbit-changing capabilities of Lorentz spacecraft; the Lorentz-force propulsion (and, therefore, the maneuvering capability) of the spacecraft is not propellant limited, so the duration and flexibility of a mission at Jupiter could be considerably increased despite the possible need for dual-propulsion systems. The figure also includes a star that marks the approximate arrival condition of the Galileo spacecraft at Jupiter, discussed in the next section.

Retrograde equatorial capture warrants some brief attention. The choice of sign in Eq. (6) that $\dot{\phi} > 0$ implicitly assumes that the incoming hyperbola is prograde. If we switch the sign of $\dot{\phi}$, then

$$\dot{p} = -2(qB_0/p^2)e \sin\nu(1 + e\cos\nu)^2 \tag{38}$$

where

$$\mathrm{d}\,e/\mathrm{d}\bar{p} = [1/(2e\bar{p})][(1 - e^2) - \bar{p}^{3/2}] \tag{39}$$

via division by Eq. (7) and conversion to nondimensional units. Equation (39) has the solution

$$e(\bar{p}) = \sqrt{1 - (2/5)\bar{p}^{3/2} + C\bar{p}} \tag{40}$$

where the constant of integration,

$$C = \bar{p}_0[(2/5)\bar{p}_0^{3/2} + e_0^2 - 1] \tag{41}$$

Unfortunately, the replacement of Eq. (11) with Eq. (40) while attempting to simultaneously solve for $\bar{p}$, e, and $\bar{r}_p$ at periapsis leads to a sextic polynomial, which does not have a general solution. Nonetheless, the approximation techniques used in Eqs. (32a–32c), to solve for the orbital elements at periapsis, remain valid, and an expression for the minimum capture charge can be derived. Because the velocity at periapsis is high for both prograde and retrograde hyperbolic orbits (often tens of kilometers per second), a retrograde capture does not necessarily lead to a significant advantage in relative velocity. At Earth, the difference in relative velocity between prograde and retrograde captures is only about 10% and, at Jupiter, 50%. The general character and placement of contours in Fig. 4 do not change substantially. A 50% gain in relative velocity appears attractive, but the increase in the Lorentz force is negligible compared with the orders of magnitude uncertainty in feasible specific charge, which translates into similar uncertainty in feasible Lorentz force. Because the coupling between orbital elements does not differ greatly between prograde and retrograde orbits, and because the higher velocity of retrograde orbits ultimately does not introduce any significant advantage from a feasibility perspective, the rest of this analysis considers exclusively prograde orbits.

Application at Jupiter

Capture Propagation and Comparison to Analytical Theory

To illustrate the results in Fig. 4, we consider a Galileo-like approach to Jupiter. The arrival v_∞ of the spacecraft is approximately 6 km/s, [29] and the initial periapsis is at 4 R_J [30]. Following the contours for the Jupiter case in Fig. 4 (Galileo is marked with a star), these initial conditions correspond to a contour where $q \approx 0.2$ C/kg. Exact evaluation of Eq. (37) for $r_{p0} = 4R_J$ ($\bar{r}_{p0} = 1.787$) and $v_\infty = 6$ km/s ($\gamma = 0.045$) finds $\delta > 0.041$ ($q > 0.186$) for capture. Therefore, for a Galileo-like arrival at Jupiter, a Lorentz spacecraft would need to generate $q > 0.186$ C/kg of specific charge (an infeasible value) during the first flyby to ensure capture. Capture into a 200-day orbit (similar to the Galileo mission profile) requires $q \approx 0.25$ C/kg, as can be calculated roughly from the work-energy theorem in Eq. (22). After capture has occurred, the specific charge can be reduced significantly, if necessary, while the orbit is lowered to an operational altitude.

Although we consider 0.2 C/kg an infeasible specific charge, a Galileo-like arrival that requires such a charge serves as an adequate baseline to test the validity of the analytical theory. To accommodate more feasible specific charges, capture would require lower initial v_∞ (0–2 km/s, per Fig. 4); although a ballistic trajectory cannot achieve less than ∼5 km/s of v_∞ (from a Hohmann transfer), various low-thrust trajectories could allow for arrival speeds this low [31]. The contours in Fig. 4 indicate that choosing a lower periapsis also lowers the charge necessary to capture. For example, a specific charge of ∼0.05 C/kg captures at $r_p \approx 1R_J$ (similar to the planned Juno mission to Jupiter, which is designed to fly just above the planet's cloud tops [32]), notwithstanding the feasibility of such a flyby, which may depend on the Lorentz spacecraft architecture. However, periapses below the synchronous radius tend to have $K > -3$ that, from Table 2, implies that periapsis falls during subsequent postcapture orbits, leading quickly to impact with the planet. A small periapsis-raise maneuver could be performed postcapture at apoapsis to offset the falling periapsis and to enable continued use of the low specific charge; we have elected not to include any propulsive maneuvers in our capture model and, therefore, do not use a baseline orbit where $K > -3$. A specific charge of 0.2 C/kg is just sufficient for capture from a Galileo-like arrival, but the first orbit postcapture would be nearly parabolic with a very high apoapsis (i.e., the orbit period approaches infinity). To increase the effectiveness of the capture and to reduce the period of the first orbit, we use a lower periapsis, 3 R_J, in the numerical example. The specific charge follows the bang–off control,

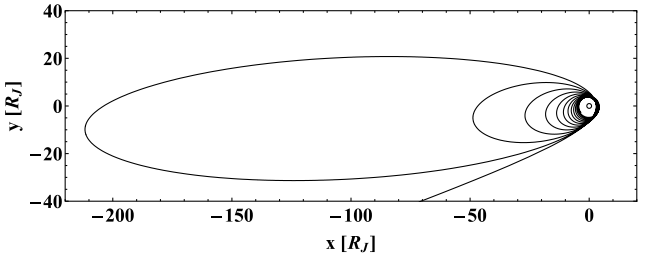

Fig. 5 An example of a propellantless capture trajectory for a Lorentz spacecraft at Jupiter.

$$q = \begin{cases} +0.2 \text{ C/kg} & \text{for } \dot{r} < 0 \\ 0 & \text{for } \dot{r} > 0 \end{cases} \tag{42}$$

so that the charge remains on while the spacecraft is inbound and turns off after crossing the line of apsides. Atchison and Peck [15] use the opposite control for their captures at Jupiter, turning on a negative charge while the spacecraft ascends. Figure 5 shows a plot of the trajectory of a Lorentz spacecraft capture at Jupiter, propagated according to the equations of motion in Eqs. (3a–3c) and using the initial conditions listed in Table 4.

The propagation begins at several thousand Jupiter radii to simulate an arrival from infinity. We do not model the gravity of the sun or of other bodies besides Jupiter, so we neglect the perturbations that arise outside of Jupiter's sphere of influence. The propagation time for the entire simulation is 1.75 years; however, two thirds of that time is spent on the incoming hyperbola from interplanetary space. The capture event and the orbit-lowering process with the Lorentz force requires 200 days. The Lorentz spacecraft approaches Jupiter from the lower left in Fig. 5. After the first flyby and capture, the spacecraft is on an orbit with a period of ∼140 days. It continues to employ the control law in Eq. (42) after the orbit becomes elliptical.

Figure 6 presents a plot of the numerically propagated eccentricity and of the eccentricity according to Eq. (11) versus time, where the numerically propagated semilatus rectum (evaluated from the state vectors) is used as the input for Eq. (11). The apparent discontinuities in the plot of eccentricity occur during periapsis passes, when the Lorentz force is at its strongest and the charge is switched off instantaneously. The difference between the numerical and analytical eccentricity calculations is too small to see on the plot; we include a plot of the percent error between the two (where the numerical eccentricity is considered the true value). The percent error is small (a fraction of a percent) for most of the propagation. As the orbit circularizes toward the end and the Lorentz spacecraft spends more time near the planet, the error increases toward 0.01%. The plot of percent error in Fig. 6 does not compare with commanded versus actual states, as in the case of testing the efficacy or stability of a control. Rather, the plot compares the analytical theory's prediction of the eccentricity's time evolution against a numerical integration of the eccentricity. The control law is intended only to circularize the orbit over several revolutions and not to control the eccentricity or any other orbital element at all times, and the control succeeds in bringing the eccentricity very close to zero over the 600-day propagation. The increase in percent error at the end of the propagation arises from the nonlinearities that grow in effect in the low circular orbits (because of higher orbital velocities that strengthen the Lorentz force beyond a small perturbation), but that the analytical theory does not account for. Nonetheless, the close absolute agreement between the numerical propagation and Eq. (11) throughout the propagation supports the analytical theory.

Table 4 Initial conditions of capture example

Parameter	Value
r_0	3500 R_J
v_∞	6 km/s
r_{p0}	3 R_J
Propagation time	640 days

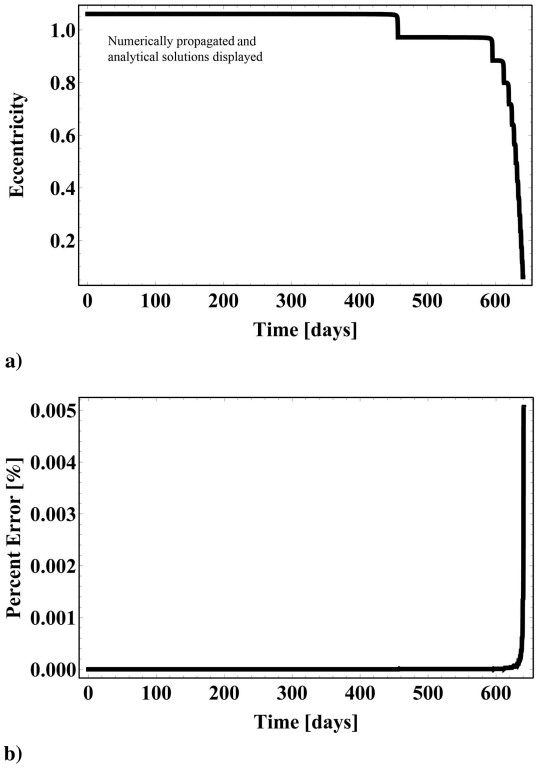

Fig. 6 The numerically integrated eccentricity and the analytical eccentricity of Eq. (11): a) displayed, which are too close to differentiate and b) a plot of the magnitude of the percent error between the two, where the numerical integration is taken as true.

Orbit Circularization

The bang–off control slowly reduces the semilatus rectum during each pass, and the eccentricity reduces accordingly via Eq. (11) (where, in this example, $K = -3.279$). These initial conditions correspond to a circularizable orbit in Fig. 3. Figures 5 and 6 show that the orbit circularizes as the trajectory propagates, although the circularization itself is asymptotic, requiring (in theory) an infinite amount of time with the given control. Atchison and Peck observed this asymptotic circularization of capture orbits in their numerical propagations and characterized these circular orbits as undesired equilibria [15]. However, Eq. (6) shows that $\dot{p}$ is directly proportional to $\dot{r}$, so as the orbit circularizes, $\dot{r} \to 0$; therefore, $\dot{p} \to 0$. The control law switches on the sign of $\dot{r}$ and explicitly reduces p through Eq. (6); as the orbit approaches circular, the charge has less and less effect because $\dot{r}$ approaches zero. A different control law that, for example, depends on ϕ, would not have this effect on $\dot{p}$, because that variable does not uniformly approach zero as the orbit circularizes. In that case, the orbit would circularize, and then the eccentricity and semilatus rectum would begin increasing in tandem (ultimately toward an escape condition if the propagation were continued). The circular orbits are not equilibria per se, but are instead an artifact of the control law and can be avoided if necessary.

Figure 7 shows contours of the radii of these asymptotic circular orbits as a function of v_∞ and r_p at Jupiter. They were evaluated by setting Eq. (11) equal to zero, solving for $\bar{p}$, and expressing the variables in dimensional form. The contours correspond to the orbital radii of the four Galilean moons: Io, Europa, Ganymede, and Callisto. The circular orbit contours depend strongly on r_{p0}, with some v_∞ dependence at high r_{p0}. Atchison and Peck's approach uses a high specific charge to reach a Galilean moon's orbital radius in only one pass of the planet [15]. We propose an alternative, where the arrival conditions could be targeted per Fig. 7 to lead asymptotically

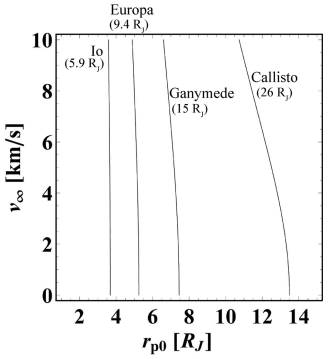

Fig. 7 Contours of asymptotic circular orbit radii as a function of initial radius of periapsis and v_∞.

to an orbit matching with a Galilean moon after many orbits. Use of the control in Eq. (42) guarantees the existence of these asymptotic orbits by virtue of the $\dot{r}$ dependence of the bang–off scheme. The magnitude of the charge does not affect the size of the final orbit; the final orbit radius is derived from Eq. (11), which is charge independent. A Lorentz spacecraft could capture into orbit about Jupiter from an arrival hyperbola corresponding to a contour in Fig. 7, reduce the magnitude of the specific charge to reduce power demands on the spacecraft, and then allow the bang–off control to asymptotically ease the spacecraft into a matching orbit of the destination moon. Phasing issues between the spacecraft and moon can be overcome by noting that the Lorentz spacecraft velocity in the asymptotic circular orbit is either subcircular or supercircular (while the charge is on) and can be controlled by judicious choice of specific charge magnitude [4]. The small differential velocity allows the moon to gradually catch up to the spacecraft (or vice versa) with a small v_∞ with respect to the moon, potentially obviating the need for complicated endgame scenarios that involve many satellite flybys to arrive at a Galilean moon [33,34].

As seen in Fig. 3, the final outcome of the capture process depends on the circularizability of the initial hyperbola. If the initial hyperbola is circularizable, the Lorentz force eventually transforms the orbit to circular (if the spacecraft is following the half-orbit bang–bang or bang–off controls); if not, the Lorentz force tends to decrease the radius of periapsis until the spacecraft impacts the planet (as per Table 2, because noncircularizable orbits have $K > -3$). Plots identifying the capture regions for Jupiter were created numerically by Atchison and Peck via the integration of 1280 initial orbits for each of four different specific charge levels [15], an example of which appears at the left in Fig. 8. That example plot (one of four from Atchison and Peck's original paper) is for the $q = 0.01$ C/kg case, where the ordinate uses the absolute value of the semimajor axis, allowing for both elliptical and hyperbolic orbits in the same quadrant. The crash region in each plot is nearly identical in size and shape for the $q = 0.001$, 0.01, and 0.1 C/kg cases; the other hatched regions correspond to orbits that either naturally circularize or achieve some eccentric state at the end of the integration time limit (i.e., 5 years).

On the right of Fig. 8, Fig. 3 has been reproduced by including only the bold threshold line ($K = -3$), which separates circularizable and noncircularizable orbits, and by reexpressing its solution [via Eq. (11)] in terms of the semimajor axis instead of the semilatus rectum. All of the orbits to the right of the dashed line fail to capture and fly by the planet (the line is not exactly on $e = 1$, so there are some orbits with eccentricity slightly higher than one that can capture using $q = 0.01$ C/kg). The flyby cases were evaluated by solving for the set of initial conditions, where $e > 1$ at periapsis.

Using the semimajor axis instead of the semilatus rectum creates an asymptote as $e \to 1$, because the solution for the semimajor axis involves divisions by zero at the parabolic orbit. Comparing the two plots in Fig. 8, the bold circularizability threshold neatly corresponds to the crash boundary found numerically. Atchison and Peck selected a crash condition of $r_p \leq 2R_J$, and the contour of this radius of periapsis very closely resembles the bold line, as demonstrated by the thin line in the analytical plot at right; however, the choppiness of the edges of the numerically evaluated crash region suggests that orbits other than just those initially with $r_p \leq 2R_J$ evolve to satisfy the crash condition. The bold circularizability threshold extends slightly beyond the $r_p = 2R_J$ contour, encompassing some initially acceptable orbits that crash after some time. Therefore, the impact region does not necessarily depend, as Atchison and Peck suggested [15], on the radius of periapsis, the contours of which do bear some resemblance to the circularizability threshold. Instead, for noncircularizable orbits, after the capture event, the Lorentz force continues to reduce the semilatus rectum; inevitably, because the orbital eccentricity cannot reach zero and freeze the orbit, the semilatus rectum is driven smaller and smaller until the periapsis shrinks to within the planet. The independence of the circularizability threshold with respect to charge magnitude and planetary magnetic properties also explains why the impact region is the same for the three numerically integrated cases with three different orders of magnitude of charge. (When $q = 1$ C/kg, the fourth case of Atchison and Peck, the plot of numerically integrated data does diverge from the analytical theory, but we would expect such divergence with high specific charge at Jupiter.) The dashed line bounding orbits that fail to capture does depend on the specific charge; the line shifts to the right as the charge increases.

All orbits outside the circularizability threshold approach the asymptotic circular orbits [if the Lorentz spacecraft is following the control law of Eq. (42)] or can be circularized in some manner. Atchison and Peck [15] have used a control similar to Eq. (42) in their

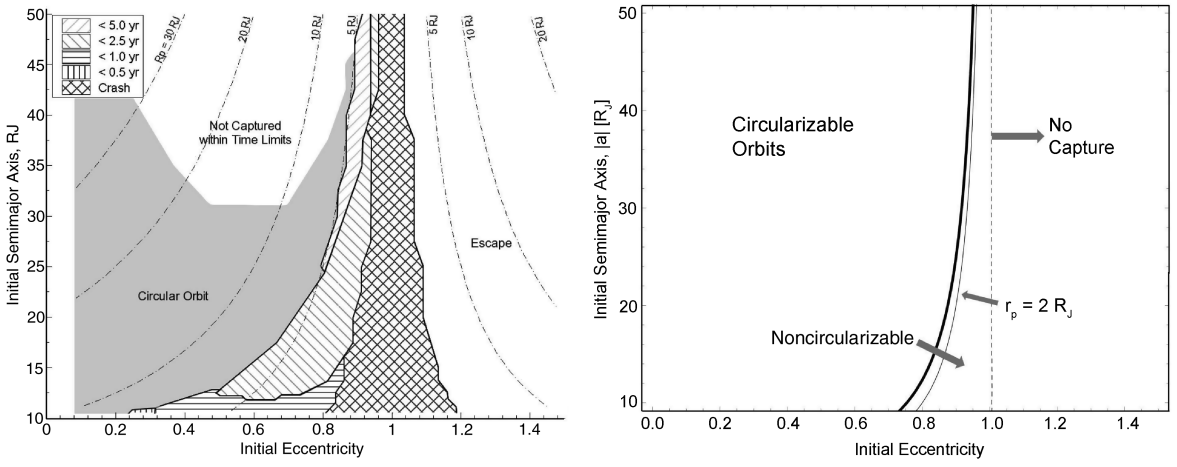

a) b)

Fig. 8 Regions at Jupiter a) identifying capture, circularization, or impact from initial orbits, numerically integrated by Atchison and Peck [15] (used with permission), and b) drawn and labeled according to the new analytical theory.

numerical integrations, which leads to the circular orbit regions on their plot; orbits in the hatched regions did not circularize within the time limits of their integration, or the integration was stopped early. The analytical theory, as supported by Fig. 8, suggests that, if the numerical integrations extended long enough, all of these elliptical orbits to the left of the crash region in Fig. 8 would eventually circularize.

Discussion

Throughout this paper, we have considered the Lorentz force alone and have neglected other possible perturbations on the Keplerian orbit, such as gravity harmonics and moons. Long-term missions with a Lorentz spacecraft could be substantially influenced by these forces, but in the case of propellantless capture considered here, the spacecraft spends little time near the planet or near any moons. An application of Lorentz spacecraft stationkeeping at Enceladus was found to be mostly unaffected by the gravitational influences of other Saturnian moons, including Titan [4]. In fact, the large orbits postcapture would be more substantially affected by the sun than by other gravitational influences [35]. We have not included the solar influence, because its importance can vary widely among specific missions and was beyond the scope of specifically characterizing the effect of the Lorentz force on Keplerian orbits.

Most planetary magnetic dipoles in the solar system have a tilt (with the exception of Saturn [28]) that alters the magnetic field gradient in the equatorial plane from the uniformity assumed in this work. However, the effect of a tilt has been shown in numerical simulations [7] to be small and, analytically, to be a second-order effect [3], so that at Jupiter, where the tilt is approximately 11 deg, we would not expect a substantial deviation from the trajectories in this paper were the tilt included. Most of the additional induced motion would be out of plane. Prior investigations have found that motion to be periodic or to induce only a small (few degree) inclination change in the type of applications considered here [4,6], and it may be possible to mitigate the effect entirely with the application of feedback control, as discussed by Streetman and Peck [7]. A secular change in the out-of-plane position of a Lorentz spacecraft is possible [5], and the behavior of inclined orbits during capture and escape has been considered elsewhere [3]. We have neglected higher harmonics of the magnetic field and multipole effects, because they would have unnecessarily detracted from the analytical results, which are intended to provide first-order insight into the effect of the Lorentz force.

While the comparison of the numerically integrated trajectory with the analytical expressions in Fig. 6 shows excellent agreement, we have observed that the initial starting radius of the numerical integration can substantially alter the apparent performance of the analytical results. The closed-form solutions in Eqs. (11) and (40) were developed assuming the ideal condition of an arrival from infinity. Because no numerical integration can begin at true infinity, a balance had to be struck between the fidelity of the integration and computation times. The initial radius of 3500 R_J was settled on as an acceptable compromise between reproducing the initial conditions of the analytical theory and the total integration time. The example trajectory in Fig. 5 already required some 1.5 years for the Lorentz spacecraft to reach its first periapsis and achieved the match with analytical theory at the precision in Fig. 6. Further fine tuning of the integration's initial conditions would have lent little or no more precision of consequence, considering the simplifying assumptions that have already been made.

Atchison and Peck [15] and Streetman and Peck [16] considered a direct-to-destination mission design that used a very high specific charge (e.g., >1 C/kg) to capture the Lorentz spacecraft into its final orbit in only one pass of the planet. Although such a strategy is time optimal to arrive at the desired final orbit, the charge-generation demands on the spacecraft are extreme. Alternatively, the spacecraft could use a specific charge, as determined by Fig. 4, to capture and then use a much lower specific charge to gradually modify the elliptical orbit according to the contours of Fig. 3 and to achieve the desired final state. This method of orbit insertion reduces the time requiring a very high charge (to only during the first flyby). Many hardware challenges remain to mitigate the deleterious effects of a high electrostatic charge. The onetime use of high specific charge in a nearly impulsive fashion at periapsis may provide the option of the spacecraft entering a safe mode during the capture event. During this time, most other systems could be temporarily deactivated or shielded for the duration of the Lorentz maneuver.

Application of the Lorentz capture and asymptotic circularization for missions at the Galilean moons of Jupiter (or, similarly, for moons of Saturn) remains speculative. Building on the results of Atchison and Peck [15] and Streetman and Peck [16], asymptotic circularization of a Lorentz spacecraft orbit offers a possible option for insertion at a Galilean moon that could require less charge to enter the final orbit and could, in fact, require little numerical targeting beyond the hyperbolic arrival conditions (to specify the final asymptotic circular orbit). However, in practice, such a mission would be beleaguered by gravitational perturbations from the target moon. As the orbit reaches a nearly circular state, the Lorentz spacecraft may repeatedly encounter the moon at altitudes low enough to qualify as flybys, substantially changing the orbital elements. Toward the end of the orbit-lowering process with the Lorentz force, a mission designer would likely need to adopt a second method to assess the near-moon and capture phases.

ED tethers have been proposed for capture and orbit maintenance at Jupiter by a number of researchers [21–23]. ED tethers are propelled by the Lorentz force in the same manner as a Lorentz spacecraft, but the tether's electric current vector (instead of the vehicle's velocity, in the case of Lorentz spacecraft) is crossed with the magnetic field. The production of the Lorentz force by the current in the tether introduces an additional degree of freedom to the propellantless maneuver problem, because the orientation of the tether can be arbitrary. However, the Lorentz force must still act perpendicularly to the tether, and modulation of the force would require quick actuation of the tether's orientation, which is not always possible. For an electrostatically charged spacecraft, the Lorentz force is constrained to act in a direction perpendicular to the velocity and the magnetic field. However, the orientation dependence of the Lorentz force in an ED tether couples the attitude and orbital dynamics, greatly complicating the analysis and requiring sophisticated control for stabilization. If a passive stabilization method, such as gravity-gradient stabilization, is employed, then the tether problem is reduced to a single scalar control (the current), the same as with the Lorentz spacecraft.

Capture at Jupiter would require an ED tether tens to hundreds of kilometers long, with the capacity to withstand hundreds of kilovolts of induced potential and many megawatts of generated power [22]. The materials that can withstand such conditions and be appropriate for space travel are an area of active research. Although hardware development for electrostatically charged spacecraft is in its infancy, several performance comparisons between Lorentz spacecraft and ED tethers have entered the literature based on preliminary power- and hardware-sizing estimates [4,7,12,15]. At specific charges similar to those considered here for Jupiter capture ($\sim$0.03 for those studies) with a 50 kg payload, a Lorentz spacecraft would require approximately 2 kW of power and 40 kV of electric potential [15]. These results depend partially on the local plasma environment and on the density of the power system. The Lorentz spacecraft often compares favorably or on par with ED tethers in power and voltage, and it has been found that a Lorentz spacecraft may, in fact, contend with traditional low-thrust propulsion systems in terms of operational lifetime [4]. Despite having fewer degrees of freedom, electrostatically charged Lorentz spacecraft remain an attractive option for future study as a complement to ED tethers, and they offer advantages from analytical and operational perspectives because of their potentially compact construction.

Conclusions

Many applications of the Lorentz force for propulsion have proved to be potent in their orbit-changing capability but, frequently, those applications were studied as individual cases via numerical

integration or through broad numerical searches of the parameter space. The analytical relationship between orbital eccentricity and semilatus rectum derived here provides a complete solution to the problem of propellantless (equatorial) capture with Lorentz spacecraft. Knowledge of the orbital elements' relative evolution offers immediate qualitative insight into the capture problem; for example, whereas earlier investigations into escape and capture have sought charge-control laws on a case-by-case basis, it is now possible to identify entire sets of orbits into which capture is impossible regardless of the choice of control. Applied to the three planets bearing significant and nearly dipolar magnetic fields (Earth, Jupiter, and Saturn), the minimum specific charges necessary to effect capture have been identified given a wide range of likely arrival conditions. Because of the currently immature state of Lorentz spacecraft hardware, Jupiter is the only promising candidate for propellantless capture in the next few decades. A numerical example of capture performed at Jupiter validated the analytical theory to a very high precision, and the analytical theory succeeds in reproducing trends and constraints on Jupiter capture orbits that were identified numerically by other investigators. This work characterizes the first-order effects of the Lorentz force acting on an electrostatically charged spacecraft during capture and demonstrates that analytical solutions are not only available in this dynamically complicated system, but they can also predict the evolution of the system with great accuracy and without the need for computationally expensive integration.

Acknowledgments

The first author is supported by a fellowship from the National Defense Science and Engineering Graduate Fellowship Program. The second author is supported in part by the Purdue Forever Fellowship. Our thanks to Justin Atchison and to Mason Peck of Cornell University for permission to reproduce their figure.

References

[1] Larson, W. J. and Wertz, J. R. (eds.), *Space Mission Analysis and Design*, 2nd ed., Microcosm, Torrance, CA, 1992, pp. 198–199, Chap. 8.1.1.

[2] Peck, M. A., "Prospects and Challenges for Lorentz-Augmented Orbits," AIAA Guidance, Navigation, and Control Conference, AIAA Paper 2005-5995, Aug. 2005.

[3] Gangestad, J. W., Pollock, G. E., and Longuski, J. M., "Lagrange's Planetary Equations for the Motion of Electrostatically Charged Spacecraft," *Celestial Mechanics and Dynamical Astronomy*, Vol. 108, No. 2, 2010, pp. 125–145. doi:10.1007/s10569-010-9297-z

[4] Gangestad, J. W., Pollock, G. E., and Longuski, J. M., "Propellantless Stationkeeping at Enceladus via the Electromagnetic Lorentz Force," *Journal of Guidance, Control, and Dynamics*, Vol. 32, No. 5, 2009, pp. 1466–1475. doi:10.2514/1.42769

[5] Pollock, G. E., Gangestad, J. W., and Longuski, J. M., "Inclination Change in Low-Earth Orbit via the Geomagnetic Lorentz Force," *Journal of Guidance, Control, and Dynamics*, Vol. 33, No. 5, 2010, pp. 1387–1395. doi:10.2514/1.48610

[6] Pollock, G. E., Gangestad, J. W., and Longuski, J. M., "Analytical Solutions for the Relative Motion of Spacecraft Subject to Lorentz-Force Perturbations," *Acta Astronautica*, 2010 (in press). doi:10.1016/j.actaastro.2010.07.007

[7] Streetman, B., and Peck, M. A., "New Synchronous Orbits Using the Geomagnetic Lorentz Force," *Journal of Guidance, Control, and Dynamics*, Vol. 30, No. 6, 2007, pp. 1677–1690. doi:10.2514/1.29080

[8] Cosmo, M. L. and Lorenzini, E. C. (eds.), *Tethers in Space Handbook*, 3rd ed., NASA, 1997.

[9] Tikhonov, A. A., "A Method of Semipassive Attitude Stabilization of a Spacecraft in the Geomagnetic Field," *Cosmic Research (Translation of Kosmicheskie Issledovaniya)*, Vol. 41, No. 1, 2003, pp. 63–71. doi:10.1023/A:1022355730291

[10] Schaub, H., Parker, G. G., and King, L. B., "Challenges and Prospects of Coulomb Spacecraft Formations," *AAS John L. Junkins Astrodynamics Symposium*, American Astronautical Society Paper 03-278, Springfield, VA, 2003.

[11] Choiniere, E., and Gilchrist, B. E., "Self-Consistent 2-D Kinetic Simulations of High-Voltage Plasma Sheaths Surrounding Ion-Attracting Conductive Cylinders in Flowing Plasmas," *IEEE Transactions on Plasma Science*, Vol. 35, No. 1, 2007, pp. 7–22. doi:10.1109/TPS.2006.889300

[12] Atchison, J., and Peck, M. A., "Dynamics and Feasibility of a Millimeter-Scale Lorentz-Propelled Satellite," AIAA Guidance, Navigation, and Control Conference, AIAA Paper 2007-6847, Aug. 2007.

[13] Seubert, C. R. and Schaub, H., "One-Dimensional Position Feedback Control Experiments Using the Coulomb Testbed," *AAS/AIAA Astrodynamics Specialist Conference and Exhibit*, American Astronautical Society Paper 09-390, Springfield, VA, 2009.

[14] Peck, M. A., Streetman, B., Saaj, C. M., and Lappas, V., "Spacecraft Formation Flying Using Lorentz Forces," *Journal of the British Interplanetary Society*, Vol. 60, 2007, pp. 263–267. doi:10.2514/1.38406

[15] Atchison, J. A. and Peck, M. A., "Lorentz-Augmented Jovian Orbit Insertion," *Journal of Guidance, Control, and Dynamics*, Vol. 32, No. 2, 2009, pp. 418–423.

[16] Streetman, B., and Peck, M. A., "Gravity-Assist Maneuvers Augmented by the Lorentz Force," *Journal of Guidance, Control, and Dynamics*, Vol. 32, No. 5, 2009, pp. 1639–1647. doi:10.2514/1.35676

[17] Garrett, H. B. and Whittlesey, A. C., "Spacecraft Charging: An Update," *IEEE Transactions on Plasma Science*, Vol. 28, No. 6, 2000, pp. 2017–2028. doi:10.1109/27.902229

[18] Longuski, J. M., Todd, R. E., and Koenig, W. W., "Survey of Nongravitational Forces and Space Environmental Torques: Applied to the Galileo," *Journal of Guidance, Control, and Dynamics*, Vol. 15, No. 3, 1992, pp. 545–553. doi:10.2514/3.20874

[19] Horanyi, M., Burns, J. A., and Hamilton, D. P., "The Dynamics of Saturn's E Ring Particles," *Icarus*, Vol. 97, No. 2, 1992, pp. 248–259. doi:10.1016/0019-1035(92)90131-P

[20] Schaffer, L., and Burns, J. A., "Charged Dust in Planetary Magnetospheres: Hamiltonian Dynamics and Numerical Simulations for Highly Charged Grains," *Journal of Geophysical Research*, Vol. 99, No. A9, 1994, pp. 211–223. doi:10.1029/94JA01231

[21] Gallagher, D. L., Johnson, L., Moore, J., and Bagenal, F., "Electrodynamic Tether Propulsion and Power Generation at Jupiter," NASA TR 1998-208475, June 1998.

[22] Williams, P., Blanksby, C., and Trivailo, P., "Tethered Planetary Capture: Controlled Maneuvers," *Acta Astronautica*, Vol. 53, Nos. 4–10, 2003, pp. 681–708. doi:10.1016/S0094-5765(03)80029-2

[23] Lorenzini, E., and Sanmartn, J., "Electrodynamic Tethers in Space," *Scientific American*, Vol. 291, No. 2, Aug. 2004, pp. 50–57. doi:10.1038/scientificamerican0804-50

[24] Vokrouhlicky, D., "The Geomagnetic Effects on the Motion of an Electrically Charged Artificial Satellite," *Celestial Mechanics and Dynamical Astronomy*, Vol. 46, No. 1, 1989, pp. 85–104. doi:10.1007/BF02426715

[25] Vokrouhlicky, D., "Lorentz Force Perturbations of the Orbit of an Electrically Charged Satellite: Case of Varying Charge," *Bulletin of the Astronomical Institutes of Czechoslovakia*, Vol. 41, No. 4, 1990, pp. 205–211.

[26] Griths, D. J., *Introduction to Electrodynamics*, 3rd ed., Prentice–Hall, Upper Saddle River, NJ, 2004, pp. 242–246.

[27] Strange, N. J. and Longuski, J. M., "Graphical Method for Gravity-Assist Trajectory Design," *Journal of Spacecraft and Rockets*, Vol. 39, No. 1, 2002, pp. 9–16. doi:10.2514/2.3800

[28] Connerney, J. E. P., "Magnetic Fields of the Outer Planets," *Journal of Geophysical Research*, Vol. 98, No. E10, 1993, pp. 18,659–18,679. doi:10.1029/93JE00980

[29] Petropoulos, A. E., Longuski, J. M., and Bonglio, E. P., "Trajectories to Jupiter via Gravity Assists from Venus, Earth, and Mars," *Journal of Spacecraft and Rockets*, Vol. 37, No. 6, 2000, pp. 776–783. doi:10.2514/2.3650

[30] Haw, R. J., Antreasian, P. G., McElrath, T. P., Graat, E. J., and Nicholson, F. T., "Navigating Galileo at Jupiter," *Journal of Spacecraft and Rockets*, Vol. 34, No. 4, 1997, pp. 503–508. doi:10.2514/2.3240

[31] Okutsu, M., Yam, C. H., and Longuski, J. M., "Low-Thrust Trajectories to Jupiter via Gravity Assists from Venus, Earth, and Mars," AIAA/

AAS Astrodynamics Specialist Conference, AIAA Paper 2006-6745, Aug. 2009.

[32] Matousek, S., "The Juno New Frontiers Mission," *Acta Astronautica*, Vol. 61, No. 10, 2007, pp. 932–939. doi:10.1016/j.actaastro.2006.12.013

[33] Kloster, K. W., Petropoulos, A. E., and Longuski, J. M., "Europa Orbiter Tour Design with Io Gravity Assists," *Acta Astronautica*, 2010 (in press). doi:10.1016/j.actaastro.2010.08.041

[34] Petropoulos, A. E., Landau, D., and Kloster, K. W., "Mission Design for the Jupiter Europa Orbiter Flagship Mission Study," *AAS/AIAA Astrodynamics Specialist Conference*, American Astronautical Society Paper 09-354, Springfield, VA, Aug. 2009.

[35] Yam, C. H., Davis, D. C., Longuski, J. M., Howell, K. C., and Buffington, B., "Saturn Impact Trajectories for Cassini End-of-Mission," *Journal of Spacecraft and Rockets*, Vol. 46, No. 2, 2009, pp. 353–364. doi:10.2514/1.38760